

Observation of high angular momentum excitons in cuprous oxide

J. Thewes,¹ J. Heckötter,¹ T. Kazimierzuk,¹ M. Aßmann,¹
D. Fröhlich,¹ M. Bayer,^{1,2} M.A. Semina,² and M.M. Glazov²

¹*Experimentelle Physik 2, Technische Universität Dortmund, D-44221 Dortmund, Germany*

²*Ioffe Institute, Russian Academy of Sciences, 194021, St.-Petersburg, Russia*

The recent observation of dipole-allowed P -excitons up to principal quantum numbers of $n = 25$ in cuprous oxide has given insight into exciton states with unprecedented spectral resolution. While so far the exciton description as a hydrogen-like complex has been sufficient for cubic crystals, we demonstrate here distinct deviations: The breaking of rotational symmetry leads to mixing of high angular momentum F - and H -excitons with the P -excitons so that they can be observed in absorption. The F -excitons show a three-fold splitting that depends systematically on n , in agreement with theoretical considerations. From detailed comparison of experiment and theory we determine the cubic anisotropy parameter of the Cu_2O valence band.

PACS numbers:

Introduction. Excitonic effects are decisive for the optical properties of semiconductors and insulators [1]. Not only leads the Coulomb interaction between an electron and a hole to a series of bound states, the *excitons*, with energies below the band gap, but also above the gap the Coulomb effects lead to a massive redistribution of oscillator strength towards the low-energy states compared to a free particle description. Due to this importance it has been a major goal to develop a detailed understanding of excitons on a quantitative level [1]. The description of the bound exciton states by the hydrogenic model has turned out to be extremely successful in this respect, in particular, for bulk semiconductors of cubic symmetry.

For excitons with wavefunction extensions much larger than the crystal unit cell (the Mott-Wannier excitons) the hydrogen formula for their binding energy, \mathcal{R}/n^2 with the Rydberg energy \mathcal{R} in a state of principal quantum number n , can be simply adapted to the solid state case by (i) changing the reduced mass of electron and proton m to that of electron and hole m^* , and (ii) screening the carrier interaction by the dielectric constant ε : $\mathcal{R}^* = \mathcal{R}m^*/(\varepsilon^2m)$. The influence of the many-body crystal environment is thus comprised in material properties that for cubic semiconductors are, as a rule, isotropic such as the scalar dielectric constant ε , leading to a formula for excitonic energies that is identical to the one in a system with rotational symmetry. The material environment typically causes a reduction of the atomic Rydberg energy by 2 – 3 orders of magnitude into the meV range.

For the hydrogen problem the spatial symmetry is determined by the continuous rotation group $\text{SO}(3)$, where the square of the orbital momentum $L^2 = l(l+1)\hbar^2$ and its z -component $L_z = m\hbar$, the magnetic quantum number, are constants of motion, making the problem integrable. Due to this symmetry the energy levels are degenerate with respect to m . For the $1/r$ -dependence of the Coulomb potential, the Lenz-Runge vector is also conserved as specific consequence of the underlying $\text{SO}(4)$ symmetry, causing the energy level degeneracy in l .

The latter degeneracy is lifted for hydrogen-like systems such as Rydberg atoms [2], where one electron is

excited into a shell with $n \gg 1$. Here the screening of the nuclear Coulomb potential by inner shell electrons causes a deviation from the $1/r$ behavior, breaking the $\text{SO}(4)$ symmetry. Phenomenologically this can be described by the quantum defect model, in which the binding energy formula is modified to $\mathcal{R}/(n - \delta_l)^2$. The quantum defect, δ_l , depends on l , as the screening varies with the angular momentum of the outmost electron state due to its different penetration into the electron core. The m -degeneracy is still maintained, though, for rotational symmetry.

In crystals this rotational symmetry is broken down to discrete groups. For bulk cubic crystals these are the groups O_h or T_d (depending on presence or absence of inversion symmetry). Since both groups represent still quite high symmetry, e.g., compared to low-dimensional semiconductors, the deviations from the rotational symmetry are usually captured solely by the lattice-periodic Bloch functions of electron and hole. The envelope wave function of Mott-Wannier excitons, however, are typically considered as hydrogen-like involving the spherical harmonics as angular momentum eigenfunctions, even though, strictly speaking, angular momentum is no longer conserved, and l, m are not good quantum numbers. So far, no indications for a failure of this description such as observation of a splitting of levels of particular l and/or mixing of levels with different l have been reported.

Due to the small Rydberg energy in prototype semiconductors of highest quality like GaAs ($\mathcal{R}^* = 4.2$ meV), consequences of the reduced crystal symmetry are hard to resolve in optical spectra of excitons. One might seek for deviations from the exciton hydrogen model in materials with larger Rydberg energy such as oxides or nitrides, for which possible exciton level splittings, however, may be blurred by crystal inhomogeneities. A somewhat unique position in terms of crystal quality is held by cuprous oxide (Cu_2O) with a Rydberg energy of about 90 meV. The high quality of Cu_2O natural crystals allowed the first experimental demonstration of excitons [3, 4], and it is evidenced also by remarkably narrow absorption lines as highlighted by the observation of the paraexciton in

magnetic field with a record linewidth below 100 neV [5].

Here we report a high resolution absorption study of the yellow exciton series in cuprous oxide. Besides the dominant P -excitons we resolve exciton triplets from $n = 4$ to 10 with linewidths in the μeV -range. These lines are ascribed to F -excitons (more precisely, to mixed F - and P -excitons). Their emergence in the spectra and their splitting which depends systematically on the principle quantum number n are consequences of the reduction from full rotational to discrete O_h symmetry. These findings are in good agreement with calculations in which the band structure details are taken into account.

Symmetry analysis. The yellow exciton series is associated with transitions between the highest valence and lowest conduction bands in Cu_2O . In this material the topmost valence band corresponds to the irreducible representation $\mathcal{D}_h = \Gamma_7^+$ of the O_h point group, and the bottom conduction band corresponds to $\mathcal{D}_e = \Gamma_6^+$, see Ref. [2] for details. The exciton wavefunction transforms according to the product $\mathcal{D}_x = \mathcal{D}_e \times \mathcal{D}_h \times \mathcal{D}_r$ where \mathcal{D}_r is the representation describing the wavefunction of the electron-hole relative motion [8].

To draw the analogy with hydrogen, it is convenient to follow the conventional description and categorize the excitonic states by the symmetry of the relative motion envelope \mathcal{D}_r . For S -excitons and P -excitons \mathcal{D}_r is irreducible, $\mathcal{D}_S = \Gamma_1^+$ and $\mathcal{D}_P = \Gamma_4^-$, respectively, while for the states with higher angular momentum, e.g. the F ($l = 3$) and H ($l = 5$) excitons the representations are reducible, $\mathcal{D}_F = \Gamma_2^- + \Gamma_4^- + \Gamma_5^-$ and $\mathcal{D}_H = \Gamma_3^- + 2\Gamma_4^- + \Gamma_5^-$, demonstrating that l is no longer a good quantum number for cubic symmetry. Still, we will maintain the exciton classification according to orbital angular momentum for simplicity.

To be optically active, the exciton state representation \mathcal{D}_x has to contain the three-dimensional $\mathcal{D}_x = \Gamma_4^-$ representation, corresponding to the components of the electric dipole operator. The product of the electron and hole Bloch functions can be decomposed as $\mathcal{D}_e \times \mathcal{D}_h = \Gamma_2^+ + \Gamma_5^+$. Taking into account the envelope function, the resulting P -excitons are optically active in one-photon transitions because Γ_4^- is contained in the product representation: $\Gamma_4^- \in \mathcal{D}_P \times \Gamma_5^+$, while this is not the case for the S - and D -excitons, so that they are dark [6]. The origin of this behavior is the even parity of conduction and valence bands in Cu_2O so that dipole transitions have to involve odd envelopes. However, accounting for the cubic crystal symmetry makes the F - and H -excitons dipole allowed in addition to the P -excitons: One can readily check that the product $\mathcal{D}_F \times \Gamma_5^+$ contains $3\Gamma_4^-$ and $\mathcal{D}_F \times \Gamma_2^+$ contains one more Γ_4^- . Hence F -exciton states can give rise to four spectral lines. However, one of those arising from the Γ_2^+ product of the Bloch functions is weak [17]. Analogously, the product $\mathcal{D}_H \times (\Gamma_2^+ + \Gamma_5^+)$ contains $5\Gamma_4^-$, hence H -exciton can give rise to five lines.

Experimentals. To test these predictions, high-resolution absorption spectra were recorded by detecting the emission of a frequency-stabilized laser with 1 neV

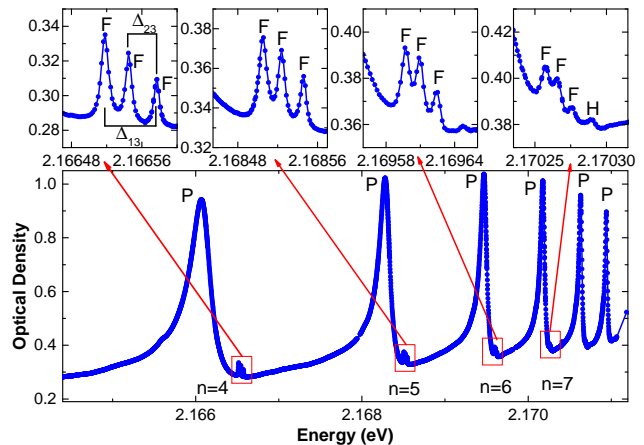


Figure 1: Bottom: absorption spectrum of the Cu_2O yellow exciton series in the energy range of states with principal quantum numbers from $n = 4$ to $n = 9$. The top panels show close-ups of the high energy flanks of the P -excitons with $n = 4, 5, 6$, and 7 , respectively. $T = 1.2$ K.

linewidth (corresponding to about 250 kHz band width) after transmission through a $30 \mu\text{m}$ thick Cu_2O crystal slab. The wavelength of the laser emission was scanned in the range of interest from 570 to 580 nm, for details see Ref. [6]. The sample was held in liquid Helium at a temperature of 1.2 K and was strain-free mounted in a holder that allowed also application of an electric field along the optical axis.

The bottom panel of Fig. 1 shows an absorption spectrum of the yellow exciton series in the energy range corresponding to principal quantum numbers from $n = 4$ to $n = 9$. The spectrum is dominated by strong absorption features of the P -excitons, discussed in detail in Ref. [6]. However, on the high energy flank of these lines weak additional features appear. We highlight that these features can be observed starting from $n = 4$ only. The top panels show close-ups of the high energy flanks of the $n = 4, 5, 6$, and 7 P -excitons. Each group of features consists of a triplet of lines with the splitting between them decreasing systematically with increasing n . The width of each line is in the μeV -range, also decreasing with n which corresponds to lifetimes in the nanosecond range. Starting from $n = 6$ another feature appears on the high energy side of the triplet, approaching the triplet with increasing principal quantum number.

For $n > 7$ the triplet is too close to the P -excitons to be resolved in absolute transmission. Therefore we have applied modulation spectroscopy by recording the differential absorption with and without an electric field applied. Only a small field of 15V/cm is applied to avoid notable modifications both of absolute exciton energies as well as splittings between them. The bottom panel in Fig. 2 shows such a modulation spectrum, in which triplets can be seen up to higher principal quantum numbers. For comparison with Fig. 1, the energy range around the

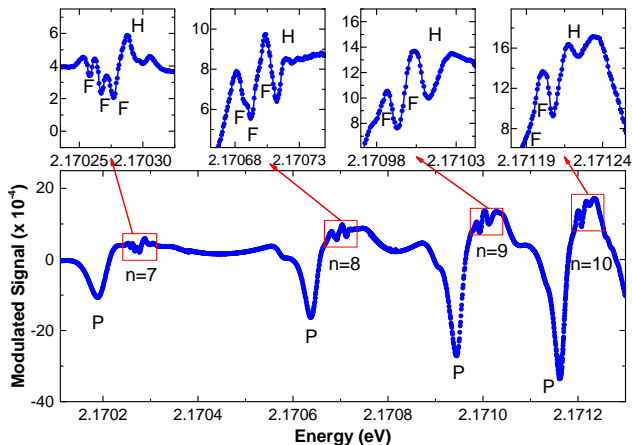


Figure 2: Modulation spectra recorded as difference of transmission spectra with and without a small electric field applied. The electric field strength is 15 V/cm. The bottom panel shows the spectral range of excitons from $n = 7$ up to 10; the top panels give close-ups of the corresponding F -exciton features.

$n = 7$ exciton is shown, where one recognizes the triplet at the same energies as before. For $n = 8$, also the triplet can be seen, where however the two low energy lines have almost merged, while the high energy line is still well separated from them. For higher n only a doublet of lines can be seen, as the splitting between the low energy lines is comparable or smaller than their line widths.

The angular momentum of exciton states belonging to a particular n is limited by $n - 1$, hence, in the hydrogen model the F -states appear only for $n \geq 4$. Since the observed triplet indeed emerges in Fig. 1 starting from $n = 4$ only, we therefore assign it to F -excitons. We note that based on the symmetry considerations presented above, F -excitons belonging to a particular n are expected to appear in optical spectra as a quadruplet (with one line being weak). The numerical calculations presented below confirm this and demonstrate that one of the lines is indeed substantially weaker as compared with three others. Moreover, its energy is very close to that of one strong line. For additional confirmation, experiments in moderate magnetic fields (not shown here) were carried out that demonstrate a splitting into 6 lines, in agreement with our symmetry analysis which predicts a two-fold splitting of each line in the triplet. Furthermore, the additional feature emerging from $n = 6$ onwards can be attributed to H -excitons. Their expected splitting is, however, too small to be resolved.

To the best of our knowledge, such high angular momentum exciton states including their fine structure splitting have not been resolved so far. We emphasize here that the description as a hydrogen-like complex can explain neither the optical activity of F - and H -excitons, nor their splitting. It is therefore a unique signature of the breaking of the rotational symmetry in the cubic crystal and a consequence of its discrete symmetry. For a

detailed understanding we have developed a microscopic description of the F -exciton fine structure.

Microscopic theory. In Cu_2O the excitonic Rydberg $\mathcal{R}^* \approx 90$ meV and the splitting between the Γ_7^+ and Γ_8^+ valence bands $\Delta \approx 130$ meV have the same order of magnitude. Therefore, a consistent theory of excitonic states has to be based on treating the complex valence band structure and the Coulomb interaction on the same level. Correspondingly, we follow the approach of Ref. [2] and present the exciton Hamiltonian (for zero center-of-mass wavevector) in the form

$$\mathcal{H} = \frac{p^2}{\hbar^2} - \frac{2}{r} - \frac{\mu}{3\hbar^2} \left(P^{(2)} \cdot I^{(2)} \right) + \frac{2}{3} \bar{\Delta} (1 + \mathbf{I} \cdot \mathbf{s}_h) + \mathcal{H}_c. \quad (1)$$

Here \mathbf{p} is the momentum of the relative electron-hole motion, \mathbf{I} is the angular momentum one operator acting in the basis of the orbital hole Bloch functions Γ_5^+ , and \mathbf{s}_h is the hole spin operator ($s_h = 1/2$). The energies are measured in units of the “bulk” excitonic Rydberg $\mathcal{R}^* = e^4 m_0 / (2\hbar^2 \varepsilon^2 \gamma_1')$, the distances are measured in units of the corresponding Bohr radius, $a^* = \hbar^2 \varepsilon \gamma_1' / (e^2 m_0)$, ε is the static dielectric constant, $\bar{\Delta} = \Delta / \mathcal{R}^*$ is the dimensionless splitting between the Γ_7^+ and Γ_8^+ bands, $\gamma_1' = \gamma_1 + m_0/m_e$, $\mu = (6\gamma_3 + 4\gamma_2)/(5\gamma_1')$, m_e is the conduction electron mass, and the γ_i ($i = 1, 2, 3$) are the Luttinger parameters. In contrast to Ref. [2] we include into the Hamiltonian (8) the contribution of the cubic symmetry responsible for the valence band warping [6]

$$\mathcal{H}_c = \frac{\delta}{3\hbar^2} \left(\sum_{k=\pm 4} [P^{(2)} \times I^{(2)}]_k^{(4)} + \frac{\sqrt{70}}{5} [P^{(2)} \times I^{(2)}]_0^{(4)} \right), \quad (2)$$

with $\delta = (\gamma_3 - \gamma_2)/\gamma_1'$. This extension is crucial, as our calculations show, to describe the fine structure of F -exciton states absent otherwise. The central-cell correction to the Coulomb potential as well as the short-range electron-hole exchange interaction are disregarded since for P - and F -excitons the wave function of the relative motion vanishes for coinciding electron and hole coordinates. In Eqs. (8) and (15) we use $P^{(2)}$ and $I^{(2)}$ for the second-rank irreducible components of the tensors $p_i p_j$ and $I_i I_j$, where $i, j = x, y, z$ and p_i, I_i are the Cartesian components of \mathbf{p} and \mathbf{I} , respectively. We note that the quartic terms in the dispersion, like $p_x^4 + p_y^4 + p_z^4$, which are allowed in O_h , result in a F - P -mixing and make the F -states active but do not cause their splitting.

The Hamiltonian (8) without cubic contribution \mathcal{H}_c ($\delta = 0$) has full rotational symmetry and already provides a quite accurate description of the P -exciton state energies [2]. Therefore, it is instructive to disregard \mathcal{H}_c and determine the spectrum and wavefunctions of P - and F -excitons. Moreover, the suppressed short-range electron-hole exchange interaction makes it possible to disregard the electron spin and characterize the excitons by the hole total momentum F and its z -component F_z , where $\mathbf{F} = \mathbf{J} + \mathbf{L}$ is the sum of the momentum of the hole Bloch functions $\mathbf{J} = \mathbf{s}_h + \mathbf{I}$ and the envelope function orbital momentum \mathbf{L} .

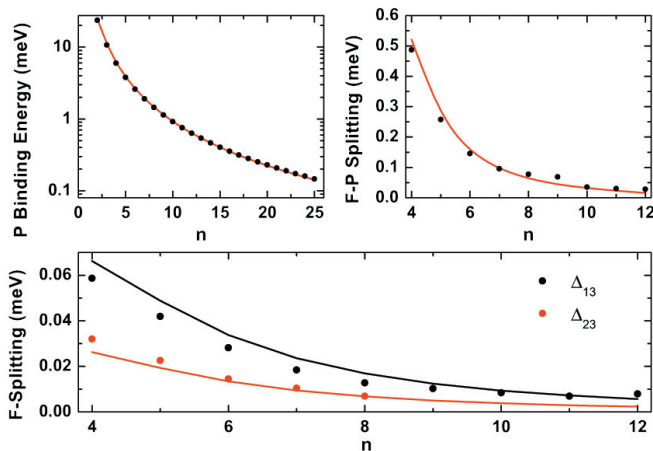


Figure 3: Comparison of theoretical calculations and experimental data for P -exciton binding energy (a), splitting between F - and P -excitons (b), and splittings of F -triplet as defined in Fig. 1 (c) vs principal quantum number. Dots give experimental data. Theory is shown by lines connecting calculated data for discrete values of n . The parameters of the calculation are: $\mathcal{R}^* = 87$ meV, $\mu = 0.47$, $\Delta = 134$ meV [2], and $\delta = -0.1$.

The P -envelopes of excitons correspond to $F = 1/2$ and $F = 3/2$ states [2], while F -excitons correspond in this approximation to $F = 5/2$ and $7/2$, respectively. Making use of its symmetry one can express the wavefunction of a state with given F via basic functions with total momentum F , $|LJF\rangle$, and radial functions $g_{LJ}(r)$, $\Psi(\mathbf{r}) = \sum_{LJ} g_{LJ}(r) |LJF\rangle$ (see Refs. [2, 4] for details), where the functions $g_{LJ}(r)$ are determined numerically following the method described in Refs. [4, 12], see Supplement [13] for details.

With inclusion of the cubic symmetry, F and F_z are no longer good quantum numbers. In particular, the $F = 5/2$ state gives rise to Γ_6^- and Γ_8^- states while $F = 7/2$ gives rise to Γ_6^- , Γ_7^- and Γ_8^- states. Note, that Γ_6^- and Γ_8^- are optically active ($\Gamma_4^- \in \Gamma_6^- \times \mathcal{D}_e$, $\Gamma_8^- \times \mathcal{D}_e$), while the Γ_7^- states are dark. States of the same symmetry have to be treated as close-to-degenerate, see Refs. [6] and [13] for details. We have calculated the energy spectrum of the P - and F -excitons for different values of the cubic anisotropy parameter δ keeping all other parameters known from literature fixed. Our calculations show that the reasonably small value of $\delta = -0.1$ gives good accord with experiment [13]. In this case two optically active states out of four have very close energies. Moreover, one of those states, namely, Γ_6^- originating from $F = 7/2$ has small oscillator strength [13]. Smaller/larger values of δ result in too small/large predictions for the F -shell splitting, so that the estimate of δ from the experimental data is quite accurate.

Discussion. Figures 3(a) and (b) compare the results of calculations of the P -exciton binding energy and the splitting between F - and P -excitons as function of principal quantum number n (the solid lines connect cal-

culated values for discrete n) with the measured data (dots), and serve as reference for the accuracy of the description of the exciton states by our model. For the F -excitons we have calculated the center-of-gravity of the F -exciton lines. The comparison shows excellent agreement between theory and experiment, providing confidence that also the μeV splittings between the F -excitons can be assessed by our model.

These splittings are shown in Fig. 3(c), where Δ_{13} is the energy separation between the outermost levels and Δ_{23} is the energy separation between the middle and higher energy level, see Fig. 1. Note, that the calculated energy of the fourth (weakly) active state coincides within the accuracy of several percent with the energy of middle state in the triplet. The points with $4 \leq n \leq 7$ were measured in absolute transmission (see Fig. 1), while points with $n \geq 8$ were taken from modulation spectroscopy. Both magnitudes of the splittings and their dependence on n are in good agreement with our calculations. The splitting between the states decreases strongly with n , as higher- n states are more extended in space so that their wave function averages over more crystal unit cells and become less sensitive to crystal symmetry deviations from the full rotation group. More quantitatively, the decrease is due to the fact that the states are intermixed by quadratic combinations of the momentum operator $p_i p_j$. The corresponding interaction matrix elements scale as the inverse square of the state radii. In the hydrogen model $\langle r^{-2} \rangle \propto n^{-3}(l+1)^{-1}$, indicating that the splittings for higher angular momentum states decrease with n and l . This explains the missing splitting of the H -excitons in absorption.

The agreement of the developed model with the experimental data allows us to accurately evaluate the valence band parameters in Cu_2O . Taking the static dielectric constant $\epsilon = 7.5$ [14], the electron effective mass $m_e = 0.99m_0$ [15], and using our values for \mathcal{R}^* , μ and δ (see text above and caption to Fig. 3), we obtain the following values of the Luttinger parameters: $\gamma_1 = 1.79$, $\gamma_2 = 0.82$, and $\gamma_3 = 0.54$. Interestingly, in this material $\gamma_3 < \gamma_2$, which is also indicated by microscopic calculations [16], see Supplement. We emphasize that the obtained Luttinger parameters may serve as benchmark for theoretical models of the Cu_2O band structure.

Conclusion. In summary, we have discovered high angular momentum exciton states in one-photon absorption spectra in high-quality Cu_2O bulk crystals. Observation of these states becomes possible through the rotational symmetry breakdown by the cubic crystal environment. Even though this symmetry breaking is weak due to the high O_h symmetry, the resulting level splittings could be resolved because of the for crystals record-low linewidths of the absorption features.

Acknowledgements. We acknowledge the support by the Deutsche Forschungsgemeinschaft and the Russian Foundation for Basic Research in the frame of ICRC TRR 160, the RF President grants MD-5726.2015.2, NSH-5062.2014.2 and NSH-1085.2014.2, Dynasty Foundation,

and programs of RAS.

- [1] See, for example, C.F. Klingshirn, *Semiconductor Optics*, Springer (2012).
- [2] See, for example, T.F. Gallagher, *Rydberg Atoms*, Cambridge Monographs on Atomic, Molecular and Chemical Physics (2005).
- [3] E.F. Gross and N.A. Karryjew, Dokl. Akad. Nauk SSSR **84**, 471 (1952).
- [4] E.F. Gross, Il Nuovo Cimento **4**, 672 (1956).
- [5] J. Brandt, D. Fröhlich, C. Sandfort, M. Bayer, H. Stolz, and N. Naka, Phys. Rev. Lett. **99**, 217403 (2007).
- [6] T. Kazimierzuk, D. Fröhlich, S. Scheel, H. Stolz, M. Bayer, *Giant Rydberg excitons in the copper oxide Cu₂O*. Nature **514**, 343 (2014).
- [7] E. L. Ivchenko. *Optical spectroscopy of semiconductor nanostructures* (Alpha Science, Harrow UK, 2005).
- [8] C. Uihlein, D. Fröhlich, R. Kenklies. *Investigation of exciton fine structure in Cu₂O*. Phys. Rev. B **23**, 2731 (1981).
- [9] S. V. Gastev, E. L. Ivchenko, G. E. Pikus, N. S. Sokolov, N. L. Yakovlev. *Polarization of paraexciton luminescence in Cu₂O crystals in magnetic field*. Fiz. Tverd. Tela **25**, 3002 (1983).
- [10] A. Baldereschi, N. O. Lipari. *Cubic contributions to the spherical model of shallow acceptor states*. Phys. Rev. B **9**, 1525 (1974).
- [11] A. Baldereschi, N. Lipari. *Spherical Model of Shallow Acceptor States in Semiconductors*. Phys. Rev. B **8**, 2697 (1973).
- [12] M. A.Semina, R. A. Suris. *Effect of localization in quantum wells and quantum wires on heavy-light hole mixing and acceptor binding energy*. Semiconductors **45**, 917 (2011).
- [13] See Supplemental Information for details
- [14] O. Madelung, U. Rössler, M. Schulz, *SpringerMaterials – The Landolt-Börnstein Database* (<http://www.springermaterials.com>) DOI: 10.1007/10681727_58.
- [15] A. Goltzene, C. Schwab, and H.C. Wolf. *Carrier resonance in Cu₂O*. Solid State Commun. **18**, 1565 (1976); J. W. Hodby, T. E. Jenkins, C. Schwab, H. Tamura, and D. Trivich. *Cyclotron resonance of electrons and of holes in cuprous oxide, Cu₂O*. J. Phys. C **9**, 1429 (1976).
- [16] E. Ruiz, S. Alvarez, P. Alemany, and R. A. Evarestov. *Electronic structure and properties of Cu₂O*. Phys. Rev. B **56**, 7189 (1997); M. French, R. Schwartz, H. Stolz, and R. Redmer. *Electronic band structure of Cu₂O by spin density functional theory*. J. of Phys.: Condens. Matt. **21**, 015502 (2009).
- [17] The transitions to the Γ_2^+ state (paraexciton) are spin-forbidden and can be activated by magnetic field [5, 9]. Owing to the cubic symmetry, the $\mathcal{D}_F \times \Gamma_2^+$ state mixes with $\mathcal{D}_F \times \Gamma_5^+$ and becomes allowed but remains weak, see Supplement for details.

SUPPLEMENTARY INFORMATION

I. SYMMETRY ANALYSIS

In the O_h point group the P -shell excitonic states (quantum number $l = 1$) transform according to the irreducible representation Γ_4^- (hereinafter we use the notations of Ref. [1]) whose basic functions can be chosen as x , y and z . The representation \mathcal{D}_3^- (F -shell states, $l = 3$) of the full spherical symmetry group, \mathcal{K}_h , is reducible in O_h and can be decomposed into the following three irreducible representations:

$$\mathcal{D}_3^- = \Gamma_2^- + \Gamma_4^- + \Gamma_5^- . \quad (3)$$

Note that in Ref. [1] the compatibility table of \mathcal{K}_h is given for the T_d group, where $\mathcal{D}_3^- = \Gamma_1 + \Gamma_4 + \Gamma_5$, so the following replacements are needed $\Gamma_1 (T_d) \rightarrow \Gamma_2^- (O_h)$, $\Gamma_4 (T_d) \rightarrow \Gamma_5^- (O_h)$ and $\Gamma_5 (T_d) \rightarrow \Gamma_4^- (O_h)$ according to the compatibility of T_d and O_h . As follows from Eq. (3) the 7-fold degenerate F -shell excitonic state splits into the singlet Γ_2^- [basic function $\propto xyz \propto Y_{3,2}(\vartheta, \varphi) - Y_{3,-2}(\vartheta, \varphi)$ (where ϑ and φ are the angles of \mathbf{r} in spherical coordinates), and two triplets Γ_4^- [basic functions transform like x^3 , y^3 , z^3 , particularly, $x^3 + iy^3 \propto \sqrt{5}Y_{3,-3}(\vartheta, \varphi) + \sqrt{3}Y_{3,1}(\vartheta, \varphi)$, $x^3 - iy^3 \propto -\sqrt{5}Y_{3,3}(\vartheta, \varphi) - \sqrt{3}Y_{3,-1}(\vartheta, \varphi)$, $z^3 \propto Y_{30}(\vartheta, \varphi)$] and Γ_5^- [basic functions like $x(y^2 - z^2)$, $y(z^2 - x^2)$, $z(x^2 - y^2)$, where, correspondingly, $x(y^2 - z^2) + iy(z^2 - x^2) \propto \sqrt{3}Y_{3,3}(\vartheta, \varphi) - \sqrt{5}Y_{3,-1}(\vartheta, \varphi)$, $x(y^2 - z^2) - iy(z^2 - x^2) \propto -\sqrt{3}Y_{3,-3}(\vartheta, \varphi) + \sqrt{5}Y_{3,1}(\vartheta, \varphi)$, $z(x^2 - y^2) \propto Y_{3,2}(\vartheta, \varphi) + Y_{3,-2}(\vartheta, \varphi)$].

With allowance for the spin and spin-orbit coupling the topmost valence band transforms according to the Γ_7^+ representation and the lowest conduction band transforms according to the Γ_6^+ representation of the O_h point symmetry group, see Ref. [2] for details. For the F -shell envelope function one has

$$\begin{aligned} \mathcal{D}_3^- \times \Gamma_7^+ \times \Gamma_6^+ &= (\Gamma_2^- + \Gamma_4^- + \Gamma_5^-) \times (\Gamma_2^+ + \Gamma_5^+) \\ &= 2\Gamma_1^- + \Gamma_2^- + 2\Gamma_3^- + 4\Gamma_4^- + 3\Gamma_5^- . \end{aligned} \quad (4)$$

Note, that Γ_4^- appears 4-times, one of these representations arises from the Γ_2^+ combination of electron and hole Bloch functions, namely,

$$\begin{aligned} |\Gamma_2^+\rangle &= -\frac{1}{\sqrt{2}}|\Gamma_6^+, -1/2\rangle|\Gamma_7^+, 1/2\rangle \\ &+ \frac{1}{\sqrt{2}}|\Gamma_6^+, 1/2\rangle|\Gamma_7^+, -1/2\rangle, \end{aligned}$$

and $\Gamma_4^- = \Gamma_5^- \times \Gamma_2^+$ with basic combinations $x(y^2 - z^2)|\Gamma_2^+\rangle$, $y(z^2 - x^2)|\Gamma_2^+\rangle$ and $z(x^2 - y^2)|\Gamma_2^+\rangle$. The Γ_2^+ representation corresponds to the paraexciton Bloch function, the transition to these Γ_4^- states is spin-forbidden, unless those states are mixed with other states of Γ_4^- symmetry.

In numerical calculations (see main text for details) it is convenient to consider the representation of the product of the hole Bloch function and the excitonic envelope, in which case we have

$$\mathcal{D}_3^- \times \Gamma_7^+ = (\Gamma_2^- + \Gamma_4^- + \Gamma_5^-) \times \Gamma_7^+ = 2\Gamma_6^- + \Gamma_7^- + 2\Gamma_8^-, \quad (5)$$

particularly,

$$\Gamma_2^- \times \Gamma_7^+ = \Gamma_6^-, \quad \Gamma_4^- \times \Gamma_7^+ = \Gamma_7^- + \Gamma_8^-, \quad \Gamma_5^- \times \Gamma_7^+ = \Gamma_6^- + \Gamma_8^-.$$

It is instructive to introduce the total momentum \mathbf{F} of the hole state, where neglecting cubic symmetry effects, states with $F = 5/2$ and $F = 7/2$ are possible for the F -shell excitons. The total angular momentum is not a good quantum number in the O_h point group, and the corresponding representations are reducible [11]:

$$\tilde{\mathcal{D}}_{5/2}^- = \Gamma_6^- + \Gamma_8^-, \quad (6a)$$

whose basic functions are (defined as in Ref. [3]):

$$\Gamma_6^- : \quad \frac{1}{\sqrt{6}}|5/2\rangle - \sqrt{\frac{5}{6}}|-3/2\rangle, \quad \frac{1}{\sqrt{6}}|-5/2\rangle - \sqrt{\frac{5}{6}}|3/2\rangle, \quad (6b)$$

$$\Gamma_8^- : \quad -\frac{1}{\sqrt{6}}|3/2\rangle - \sqrt{\frac{5}{6}}|-5/2\rangle, \\ |1/2\rangle, \quad -|-1/2\rangle, \\ \frac{1}{\sqrt{6}}|-3/2\rangle + \sqrt{\frac{5}{6}}|5/2\rangle, \quad (6c)$$

and

$$\tilde{\mathcal{D}}_{7/2}^- = \Gamma_6^- + \Gamma_7^- + \Gamma_8^-, \quad (7a)$$

with basic functions:

$$\Gamma_6^- : \quad \frac{\sqrt{3}}{2}|5/2\rangle - \frac{1}{2}|-3/2\rangle, \quad \frac{1}{2}|3/2\rangle - \frac{\sqrt{3}}{2}|-5/2\rangle, \quad (7b)$$

$$\Gamma_7^- : \quad \sqrt{\frac{5}{12}}|-7/2\rangle + \sqrt{\frac{7}{12}}|1/2\rangle, \\ -\sqrt{\frac{5}{12}}|7/2\rangle - \sqrt{\frac{7}{12}}|-1/2\rangle, \quad (7c)$$

$$\Gamma_8^- : \quad \frac{\sqrt{3}}{2}|3/2\rangle + \frac{1}{2}|-5/2\rangle, \quad \sqrt{\frac{7}{12}}|-7/2\rangle - \sqrt{\frac{5}{12}}|1/2\rangle, \quad (7d)$$

$$\sqrt{\frac{7}{12}}|7/2\rangle - \sqrt{\frac{5}{12}}|-1/2\rangle, \quad \frac{1}{2}|5/2\rangle + \frac{\sqrt{3}}{2}|-3/2\rangle.$$

The numbers in the ‘‘kets’’ denote the projections of F_z . Making use of Eq. (5) one obtains the optically active states $\Gamma_4^- \in \Gamma_6^- \times \Gamma_6^+$ and $\Gamma_4^- \in \Gamma_8^- \times \Gamma_6^+$.

The selection rules for optical transitions from the valence band states Eqs. (6a), (7) are similar to the transitions in GaAs-like semiconductors (T_d point symmetry) with the replacement $\Gamma_7(T_d) \leftrightarrow \Gamma_6^-(O_h)$.

II. COMPUTATIONAL APPROACH

To obtain the fine structure of the F -shell exciton states we follow the approach of Refs. [2, 4]. We start in the spherical approximation, which takes into account explicitly the mixing of the Γ_7^+ and Γ_8^+ valence subbands and afterwards we allow for cubic contributions.

A. Spherical approximation

Furthermore, we neglect the central-cell corrections to the electron-hole potential and the electron-hole exchange interaction. The Hamiltonian for the exciton with center of mass momentum $\mathbf{P} = 0$ has the form [cf. Eq. (1) of the main text]:

$$\mathcal{H} = \frac{p^2}{\hbar^2} - \frac{2}{r} - \frac{\mu}{3\hbar^2} \left(P^{(2)} \cdot I^{(2)} \right) + \frac{2}{3}\bar{\Delta}(1 + \mathbf{I} \cdot \mathbf{s}_h), \quad (8)$$

where p is the momentum of relative electron-hole motion, \mathbf{I} is the angular momentum one operator acting in the basis of orbital hole Bloch functions Γ_5^+ , \mathbf{s}_h is the hole spin operator ($s_h = 1/2$), the energies are measured in units of the ‘‘bulk’’ excitonic Rydberg $\mathcal{R}^* = e^4 m_0 / (2\hbar^2 \varepsilon^2 \gamma_1')$, the distances are measured in units of the corresponding Bohr radius, $a_0 = \hbar^2 \varepsilon \gamma_1' / (e^2 m_0)$, ε is the static dielectric constant, $\bar{\Delta} = \Delta / R_0$ is the dimensionless splitting between the Γ_7^+ and Γ_8^+ bands, $\gamma_1' = \gamma_1 + m_0 / m_e$,

$$\mu = \frac{6\gamma_3 + 4\gamma_2}{5\gamma_1'},$$

and γ_i ($i = 1, 2, 3$) are the Luttinger parameters.

In the spherical approximation the good quantum numbers are F and F_z , where $\mathbf{F} = \mathbf{L} + \mathbf{J}$ is the total angular momentum of the envelope, \mathbf{L} , and the hole, $\mathbf{J} = \mathbf{I} + \mathbf{s}_h$, states. The wavefunction is written as

$$\Psi(\rho) = \sum_{LJ} g_{LJ}(\rho) |LJF\rangle \\ = \sum_{LL_z, JJ_z} g_{LJ}(\rho) Y_{LL_z}(\theta, \varphi) C_{LL_z; JJ_z}^{FF_z} |J, J_z\rangle, \quad (9)$$

where $g_{LJ}(\rho)$ are the radial functions, Y_{LL_z} are the spherical harmonics, $C_{LL_z; JJ_z}^{FF_z}$ are the Clebsch-Gordan coefficients, and $|J, J_z\rangle$ are the basic functions of the valence

band top. The effective Hamiltonian acting on the radial functions can be constructed making use of the Appen-

dices of Refs. [2, 4]. Its matrix elements between the $|LJF\rangle$ and $|L'J'F'\rangle$ states read

$$\langle LJF | \left(\frac{p^2}{\hbar^2} - \frac{2}{r} \right) | L'J'F' \rangle = \delta_{LL'} \delta_{JJ'} \delta_{FF'} \left(-\frac{d^2}{dr^2} - \frac{2}{r} \frac{d}{dr} + \frac{L(L+1)}{r^2} - \frac{2}{r} \right), \quad (10a)$$

$$\langle LJF | \left(P^{(2)} \cdot I^{(2)} \right) | L'J'F' \rangle = 3\sqrt{5} \delta_{FF'} (-1)^{F+L'+J+J'+3/2} \sqrt{(2J+1)(2J'+1)} \times \quad (10b)$$

$$\left\{ \begin{matrix} L & 2 & L' \\ J' & F & J \end{matrix} \right\} \left\{ \begin{matrix} 1 & 2 & 1 \\ J & \frac{1}{2} & J' \end{matrix} \right\} (L || P^{(2)} || L'),$$

where $\left\{ \begin{matrix} a & b & c \\ d & e & f \end{matrix} \right\}$ are the $6j$ -symbols defined in Ref. [5], and

$$(L || P^{(2)} || L) = \sqrt{3} \hbar^2 \sqrt{\frac{L(2L+1)(2L+2)}{(2L-1)(2L+3)}} P_{L,L}, \quad (11a)$$

$$(L-2 || P^{(2)} || L) = -3\hbar^2 \sqrt{\frac{L(L-1)}{2L-1}} P_{L-2,L}, \quad (11b)$$

$$(L+2 || P^{(2)} || L) = -\frac{3}{2} \hbar^2 \sqrt{\frac{(2L+2)(2L+4)}{2L+3}} P_{L+2,L}, \quad (11c)$$

with

$$P_{L,L} = \frac{d^2}{dr^2} + \frac{2}{r} \frac{d}{dr} - \frac{L(L+1)}{r^2}, \quad P_{L-2,L} = \frac{d^2}{dr^2} + \frac{2L+1}{r} \frac{d}{dr} + \frac{L^2-1}{r^2}, \quad (12)$$

$$P_{L+2,L} = \frac{d^2}{dr^2} - \frac{2L+1}{r} \frac{d}{dr} + \frac{L(L+2)}{r^2}.$$

In the spherical approximation the F -exciton states correspond to total momentum $F = 5/2$ or $F = 7/2$.

Making use of Eqs. (8) and (10) we arrive at the following equations

$$F = 5/2; \quad \Psi = g_{3,1/2}(\rho) |3, 1/2, 5/2\rangle + g_{1,3/2}(\rho) |1, 3/2, 5/2\rangle + g_{3,3/2}(\rho) |3, 3/2, 5/2\rangle, \quad (13a)$$

$$\begin{pmatrix} P_{3,3} + \frac{2}{r} & \sqrt{\frac{6}{5}} \mu P_{3,1} & -\frac{2}{\sqrt{5}} \mu P_{3,3} \\ \sqrt{\frac{6}{5}} \mu P_{1,3} & (1 + \mu/5) P_{1,1} + \frac{2}{r} - \bar{\Delta} & -\frac{2\sqrt{6}}{5} \mu P_{1,3} \\ -\frac{2}{\sqrt{5}} \mu P_{3,3} & -\frac{2\sqrt{6}}{5} \mu P_{3,1} & (1 - \mu/5) P_{3,3} + \frac{2}{r} - \bar{\Delta} \end{pmatrix} \begin{pmatrix} g_{3,1/2} \\ g_{1,3/2} \\ g_{3,3/2} \end{pmatrix} = E \begin{pmatrix} g_{3,1/2} \\ g_{1,3/2} \\ g_{3,3/2} \end{pmatrix}. \quad (13b)$$

$$F = 7/2; \quad \Psi = g_{3,1/2}(\rho) |3, 1/2, 7/2\rangle + g_{3,3/2}(\rho) |3, 3/2, 7/2\rangle + g_{5,3/2}(\rho) |5, 3/2, 7/2\rangle, \quad (14a)$$

$$\begin{pmatrix} P_{3,3} + \frac{2}{r} & \frac{1}{\sqrt{3}} \mu P_{3,3} & -\sqrt{\frac{5}{3}} \mu P_{3,5} \\ \frac{1}{\sqrt{3}} \mu P_{3,3} & (1 - 2\mu/3) P_{3,3} + \frac{2}{r} - \bar{\Delta} & -\frac{\sqrt{5}}{3} \mu P_{3,5} \\ -\sqrt{\frac{5}{3}} \mu P_{5,3} & -\frac{\sqrt{5}}{3} \mu P_{5,3} & (1 + 2\mu/3) P_{5,5} + \frac{2}{r} - \bar{\Delta} \end{pmatrix} \begin{pmatrix} g_{3,1/2} \\ g_{3,3/2} \\ g_{5,3/2} \end{pmatrix} = E \begin{pmatrix} g_{3,1/2} \\ g_{3,3/2} \\ g_{5,3/2} \end{pmatrix}. \quad (14b)$$

The calculated binding energies of the P -excitons and splittings between P - and F -excitons are presented in

Fig. 3(a) and (b) of the main text. Our calculations show (see below for more details) that the splitting between the $F = 5/2$ and $F = 7/2$ F -exciton states is much smaller compared with the splitting between the F - and P -excitons. Therefore the fine structure of F excitons is not shown in Fig. 3 of the main text.

B. Effects of cubic symmetry

We follow Refs. [6, 7] and include cubic contributions to the hole Hamiltonian in the form [cf. Eq. (2) of the main text]

$$\mathcal{H}_c = \frac{\delta}{3\hbar^2} \left(\sum_{k=\pm 4} [P^{(2)} \times I^{(2)}]_k^{(4)} + \frac{\sqrt{70}}{5} [P^{(2)} \times I^{(2)}]_0^{(4)} \right), \quad (15)$$

where $\delta = (\gamma_3 - \gamma_2)/\gamma'_1$. Generally, this contribution mixes states with different F_z for given F and with different F . This is because in cubic symmetry the angular momentum is not a good quantum number. The matrix

elements of Eq. (15) can be calculated in a way similar to the derivation of Eq. (10b) and Eq. (A2) in Ref. [6]:

$$\begin{aligned} \langle L' J' F' F'_z | [P^{(2)} \times I^{(2)}]_m^{(4)} | L J F F_z \rangle \\ = 9\sqrt{5} \times (-1)^{F'-F'_z+J+3/2} \times \\ \sqrt{(2J+1)(2J'+1)(2F+1)(2F'+1)} \times \quad (16) \end{aligned}$$

$$\begin{pmatrix} F' & 4 & F \\ -F'_z & m & F_z \end{pmatrix} \begin{Bmatrix} J' & J & 2 \\ L' & L & 2 \\ F' & F & 2 \end{Bmatrix} \left\{ \begin{matrix} 1 & 2 & 1 \\ J & \frac{1}{2} & J' \end{matrix} \right\} (L || P^{(2)} || L'),$$

with the $3j$ symbols $\begin{pmatrix} a & b & c \\ d & e & f \end{pmatrix}$ and $9j$ symbols $\begin{Bmatrix} a & b & c \\ d & e & f \\ g & h & j \end{Bmatrix}$ defined in Ref. [5].

The wavefunctions of the states satisfy the following equations [12]

$$F = 5/2, \Gamma_6^-; \quad \Psi = g_{3,1/2}(\rho)|3, 1/2, 5/2, \Gamma_6^- \rangle + g_{1,3/2}(\rho)|1, 3/2, 5/2, \Gamma_6^- \rangle + g_{3,3/2}(\rho)|3, 3/2, 5/2, \Gamma_6^- \rangle, \quad (17a)$$

$$\begin{pmatrix} P_{3,3} + \frac{2}{r} & \left(\sqrt{\frac{6}{5}}\mu - \frac{8\delta}{35}\sqrt{\frac{6}{5}}\right) P_{3,1} & \left(-\frac{2}{\sqrt{5}}\mu + \frac{16\delta}{35\sqrt{5}}\right) P_{3,3} \\ \left(\sqrt{\frac{6}{5}}\mu - \frac{8\delta}{35}\sqrt{\frac{6}{5}}\right) P_{1,3} & \left(1 + \frac{\mu}{5} + \frac{24\delta}{25}\right) P_{1,1} + \frac{2}{r} - \bar{\Delta} & \left(-\frac{2\sqrt{6}}{5}\mu + \frac{2\sqrt{6}}{25}\delta\right) P_{1,3} \\ \left(-\frac{2}{\sqrt{5}}\mu + \frac{16\delta}{35\sqrt{5}}\right) P_{3,3} & \left(-\frac{2\sqrt{6}}{5}\mu + \frac{2\sqrt{6}}{25}\delta\right) P_{3,1} & \left(1 - \frac{\mu}{5} - \frac{68\delta}{175}\right) P_{3,3} + \frac{2}{r} - \bar{\Delta} \end{pmatrix} \begin{pmatrix} g_{3,1/2} \\ g_{1,3/2} \\ g_{3,3/2} \end{pmatrix} = E \begin{pmatrix} g_{3,1/2} \\ g_{1,3/2} \\ g_{3,3/2} \end{pmatrix}. \quad (17b)$$

$$F = 5/2, \Gamma_8^-; \quad \Psi = g_{3,1/2}(\rho)|3, 1/2, 5/2, \Gamma_8^- \rangle + g_{1,3/2}(\rho)|1, 3/2, 5/2, \Gamma_8^- \rangle + g_{3,3/2}(\rho)|3, 3/2, 5/2, \Gamma_8^- \rangle, \quad (18a)$$

$$\begin{pmatrix} P_{3,3} + \frac{2}{r} & \left(\sqrt{\frac{6}{5}}\mu + \frac{4\delta}{35}\sqrt{\frac{6}{5}}\right) P_{3,1} & \left(-\frac{2}{\sqrt{5}}\mu - \frac{8\delta}{35\sqrt{5}}\right) P_{3,3} \\ \left(\sqrt{\frac{6}{5}}\mu + \frac{4\delta}{35}\sqrt{\frac{6}{5}}\right) P_{1,3} & \left(1 + \frac{\mu}{5} - \frac{12\delta}{25}\right) P_{1,1} + \frac{2}{r} - \bar{\Delta} & \left(-\frac{2\sqrt{6}}{5}\mu - \frac{\sqrt{6}}{25}\delta\right) P_{1,3} \\ \left(-\frac{2}{\sqrt{5}}\mu - \frac{8\delta}{35\sqrt{5}}\right) P_{3,3} & \left(-\frac{2\sqrt{6}}{5}\mu - \frac{\sqrt{6}}{25}\delta\right) P_{3,1} & \left(1 - \frac{\mu}{5} + \frac{34\delta}{175}\right) P_{3,3} + \frac{2}{r} - \bar{\Delta} \end{pmatrix} \begin{pmatrix} g_{3,1/2} \\ g_{1,3/2} \\ g_{3,3/2} \end{pmatrix} = E \begin{pmatrix} g_{3,1/2} \\ g_{1,3/2} \\ g_{3,3/2} \end{pmatrix}. \quad (18b)$$

$$F = 7/2, \Gamma_7^-; \quad \Psi = g_{3,1/2}(\rho)|3, 1/2, 7/2, \Gamma_7^- \rangle + g_{3,3/2}(\rho)|3, 3/2, 7/2, \Gamma_7^- \rangle + g_{5,3/2}(\rho)|5, 3/2, 7/2, \Gamma_7^- \rangle, \quad (19a)$$

$$\begin{pmatrix} P_{3,3} + \frac{2}{r} & \left(\frac{\mu}{\sqrt{3}} + \frac{16\delta}{15\sqrt{3}}\right) P_{3,3} & -\left(\sqrt{\frac{5}{3}}\mu + \frac{8\delta}{33\sqrt{15}}\right) P_{3,5} \\ \left(\frac{\mu}{\sqrt{3}} + \frac{16\delta}{15\sqrt{3}}\right) P_{3,3} & \left(1 - \frac{2\mu}{3} - \frac{8\delta}{45}\right) P_{3,3} + \frac{2}{r} - \bar{\Delta} & -\left(\sqrt{\frac{5}{3}}\mu - \frac{28\delta}{99\sqrt{5}}\right) P_{3,5} \\ -\left(\sqrt{\frac{5}{3}}\mu + \frac{8\delta}{33\sqrt{15}}\right) P_{5,3} & -\left(\frac{\sqrt{5}}{3}\mu - \frac{28\delta}{99\sqrt{5}}\right) P_{5,3} & \left(1 + \frac{2\mu}{3} - \frac{56\delta}{495}\right) P_{5,5} + \frac{2}{r} - \bar{\Delta} \end{pmatrix} \begin{pmatrix} g_{3,1/2} \\ g_{3,3/2} \\ g_{5,3/2} \end{pmatrix} = E \begin{pmatrix} g_{3,1/2} \\ g_{3,3/2} \\ g_{5,3/2} \end{pmatrix}. \quad (19b)$$

$$F = 7/2, \Gamma_6^-; \quad \Psi = g_{3,1/2}(\rho)|3, 1/2, 7/2, \Gamma_6^- \rangle + g_{3,3/2}(\rho)|3, 3/2, 7/2, \Gamma_6^- \rangle + g_{5,3/2}(\rho)|5, 3/2, 7/2, \Gamma_6^- \rangle, \quad (20a)$$

$$\begin{pmatrix} P_{3,3} + \frac{2}{r} & \left(\frac{\mu}{\sqrt{3}} - \frac{16\sqrt{3}\delta}{35}\right) P_{3,3} & -\left(\sqrt{\frac{5}{3}}\mu - \frac{8\delta}{77}\sqrt{\frac{3}{5}}\right) P_{3,5} \\ \left(\frac{\mu}{\sqrt{3}} - \frac{16\sqrt{3}\delta}{35}\right) P_{3,3} & \left(1 - \frac{2\mu}{3} + \frac{8\delta}{35}\right) P_{3,3} + \frac{2}{r} - \bar{\Delta} & -\left(\frac{\sqrt{5}}{3}\mu + \frac{4\delta}{11\sqrt{5}}\right) P_{3,5} \\ -\left(\sqrt{\frac{5}{3}}\mu - \frac{8\delta}{77}\sqrt{\frac{3}{5}}\right) P_{3,5} & -\left(\frac{\sqrt{5}}{3}\mu + \frac{4\delta}{11\sqrt{5}}\right) P_{3,5} & \left(1 + \frac{2\mu}{3} + \frac{8\delta}{55}\right) P_{5,5} + \frac{2}{r} - \bar{\Delta} \end{pmatrix} \begin{pmatrix} g_{3,1/2} \\ g_{3,3/2} \\ g_{5,3/2} \end{pmatrix} = E \begin{pmatrix} g_{3,1/2} \\ g_{3,3/2} \\ g_{5,3/2} \end{pmatrix}. \quad (20b)$$

$$F = 7/2, \Gamma_8^-; \quad \Psi = g_{3,1/2}(\rho)|3, 1/2, 7/2, \Gamma_8^- \rangle + g_{3,3/2}(\rho)|3, 3/2, 7/2, \Gamma_8^- \rangle + g_{5,3/2}(\rho)|5, 3/2, 7/2, \Gamma_8^- \rangle, \quad (21a)$$

$$\begin{pmatrix} P_{3,3} + \frac{2}{r} & \left(\frac{\mu}{\sqrt{3}} + \frac{16\delta}{105\sqrt{3}}\right) P_{3,3} & -\left(\sqrt{\frac{5}{3}}\mu + \frac{8\delta}{231\sqrt{15}}\right) P_{3,5} \\ \left(\frac{\mu}{\sqrt{3}} + \frac{16\delta}{105\sqrt{3}}\right) P_{3,3} & \left(1 - \frac{2\mu}{3} - \frac{8\delta}{315}\right) P_{3,3} + \frac{2}{r} - \bar{\Delta} & -\left(\frac{\sqrt{5}}{3}\mu - \frac{4\delta}{99\sqrt{5}}\right) P_{3,5} \\ -\left(\sqrt{\frac{5}{3}}\mu + \frac{8\delta}{231\sqrt{15}}\right) P_{3,5} & -\left(\frac{\sqrt{5}}{3}\mu - \frac{4\delta}{99\sqrt{5}}\right) P_{3,5} & \left(1 + \frac{2\mu}{3} - \frac{8\delta}{495}\right) P_{5,5} + \frac{2}{r} - \bar{\Delta} \end{pmatrix} \begin{pmatrix} g_{3,1/2} \\ g_{3,3/2} \\ g_{5,3/2} \end{pmatrix} = E \begin{pmatrix} g_{3,1/2} \\ g_{3,3/2} \\ g_{5,3/2} \end{pmatrix}. \quad (21b)$$

Our calculations show that, in fact, $F = 5/2$ and $F = 7/2$ are very close to each other in energy. Therefore, we need to take into account their mixing by the Hamiltonian (15). Using the approach of Ref. [6] and Eq. (16) we obtain the following effective Hamiltonians:

$$\mathcal{H}(\Gamma_6^-) = \begin{pmatrix} \mathcal{H}(5/2, \Gamma_6^-) & \mathcal{X}_6 \\ \mathcal{X}_6^\dagger & \mathcal{H}(7/2, \Gamma_6^-) \end{pmatrix}, \quad (22a)$$

where $\mathcal{H}(5/2, \Gamma_6^-)$ and $\mathcal{H}(7/2, \Gamma_6^-)$ are given by Eqs. (17b) and (20b), respectively, and

$$\mathcal{X}_6 = \begin{pmatrix} 0 & +\frac{8\delta}{21}P_{3,3} & -\frac{4\sqrt{5}\delta}{231}P_{3,5} \\ -\frac{6\delta}{7}\sqrt{\frac{2}{5}}P_{1,3} & 0 & 0 \\ +\frac{4\delta}{7}\sqrt{\frac{3}{5}}P_{3,3} & -\frac{4\sqrt{5}\delta}{21}P_{3,3} & +\frac{4\delta}{33}P_{3,5} \end{pmatrix}, \quad (22b)$$

for the Γ_6 representation and

$$\mathcal{H}(\Gamma_8^-) = \begin{pmatrix} \mathcal{H}(5/2, \Gamma_8^-) & \mathcal{X}_8 \\ \mathcal{X}_8^\dagger & \mathcal{H}(7/2, \Gamma_8^-) \end{pmatrix}, \quad (23a)$$

where $\mathcal{H}(5/2, \Gamma_8^-)$ and $\mathcal{H}(7/2, \Gamma_8^-)$ are given by Eqs. (18b) and (21b), respectively, and

$$\mathcal{X}_8 = \begin{pmatrix} 0 & +\frac{8\delta}{7\sqrt{15}}P_{3,3} & -\frac{4\delta}{77\sqrt{4}}P_{3,5} \\ -\frac{6\sqrt{6}\delta}{35}P_{1,3} & 0 & 0 \\ +\frac{12\delta}{35}P_{3,3} & -\frac{4\delta}{7\sqrt{3}}P_{3,3} & +\frac{4\delta}{11\sqrt{15}}P_{3,5} \end{pmatrix}, \quad (23b)$$

for the Γ_8^- representation.

III. TRANSITION ENERGIES AND OSCILLATOR STRENGTHS

Figure 4 shows the energies of the F -excitons calculated according to the developed model as function of the cubic anisotropy parameter δ . The other parameters were taken from Ref. [2]. The dots give the numerical results, the states are labeled according to the representation of the hole state in Eq. (5). For $\delta = -0.1$ two

of the four F -exciton states become almost degenerate and, moreover, the values of splittings between the non-degenerate states are close to the experimental data (see also Fig. 3(c) of the main text). The absolute values of the calculated transition energies deviate slightly from the energies measured experimentally. This deviation can be corrected by minor variation of the band gap energy in our calculations.

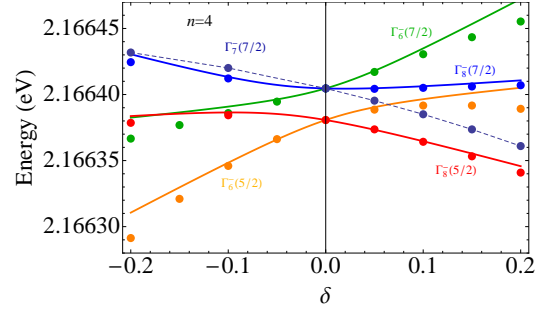


Figure 4: Calculated energies of the F -excitons for the principle quantum number $n = 4$. Dots are the results of numerical calculations, solid lines are the description in the framework of the analytical model, Eq. (24). States are labeled according to the representations of the O_h group for the hole state Eq. (5), numbers in brackets denote the total momentum F of states for $\delta = 0$. Note that the Γ_7^- state is dark. The parameters of the calculation are: $\mathcal{R}^* = 87$ meV, $\mu = 0.47$, $\Delta = 134$ meV [2]

In order to obtain more insight into the level behavior we introduce a two-level approximation valid for pairs of Γ_6^- and Γ_8^- levels for a not too large cubic anisotropy parameter δ as follows:

$$\mathcal{H} = \begin{pmatrix} E_1 + \alpha_1\delta & \beta\delta \\ \beta\delta & E_2 + \alpha_2\delta, \end{pmatrix} \quad (24a)$$

where $E_{1,2}$ are the energies of the states at $\delta = 0$, $\alpha_{1,2}$ describe the linear-with- δ shift of the diagonal energies,

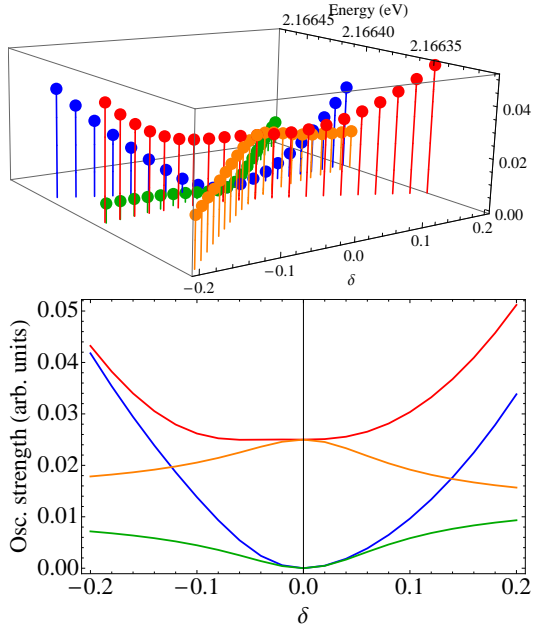


Figure 5: Energies of F -shell states and their relative oscillator strengths calculated in the framework of the two-level model, Eqs. (24). For the Γ_8^- states two contributions to the oscillator strength are taken into account, see text for details.

β describes the state mixing. The resulting energies are

$$\mathcal{E}_{1,2} = \frac{E_1 + E_2 + (\alpha_1 + \alpha_2)\delta}{2} \pm \sqrt{\left(\frac{E_1 - E_2 + (\alpha_1 - \alpha_2)\delta}{2}\right)^2 + \beta^2\delta^2}, \quad (24b)$$

and agree well with the numerical results, see the solid lines in Fig. 4.

To analyze the oscillator strengths we note that already in the spherical approximation the states Γ_8^- and Γ_6^- originating from the $F = 5/2$ level are optically active. This is because the F -shell contribution with Γ_7^+ Bloch functions is mixed with the P -shell envelope with Γ_8^+ Bloch function, see Eq. (13a).

The cubic O_h point symmetry of the cuprous oxide

crystal results in mixing of the $F = 5/2$ and $F = 7/2$ states described by Eqs. (22). This makes optical transitions from the Γ_8^- and Γ_6^- states allowed. This is the only origin of optical activity for the $\Gamma_6^-(7/2)$ state shown by the green points and lines in Figs. 4 and 5 (note also that the corresponding exciton wavefunction contains substantial contribution from the Γ_2^+ Bloch exciton state). For the Γ_8^- states additional contributions to the oscillator strength arise due to the presence of the x^3 , y^3 , z^3 -like envelopes of the Γ_7^+ Bloch functions which, as a result of e.g. quartic contributions in the free-carrier dispersion [8]

$$p_x^4 + p_y^4 + p_z^4,$$

contain P -shell contributions. This contribution enhances the oscillator strength of the $\Gamma_8^-(7/2)$ state as compared with the $\Gamma_6^-(7/2)$ state.

IV. DETERMINATION OF γ_3 SIGN FROM MICROSCOPIC BAND STRUCTURE CALCULATIONS

The analysis above, see Fig. 4 and Fig. 3 from the main text shows that the best agreement of our calculations with experiment is achieved for $\delta < 0$, i.e. for $\gamma_3 < \gamma_2$ (we recall that γ_1 , γ_2 and γ_3 are the Luttinger parameters). In order to verify this result we present in Fig. 6 the topmost valence band energies calculated by DFT in Ref. [9] and parabolic fits to these results for the directions [001] (left) and [111] (right). The accuracy of the fits is not enough to determine the values of all Luttinger parameters but the sign of the difference $\gamma_3 - \gamma_2$ can be reliably found. The estimation yields that $\gamma_3 - \gamma_2$ is negative and $(\gamma_3 - \gamma_2)/\gamma_1 \approx -0.3$ (for our parameters $(\gamma_3 - \gamma_2)/\gamma_1 = \delta\gamma'_1/\gamma_1 \approx -0.15$). The fact that $\gamma_3 < \gamma_2$ is also consistent with Ref. [10], where the DFT calculations were carried out neglecting spin-orbit coupling. In the latter case, however, the accuracy of extraction of parameters is low and a direct calculation shows that in Ref. [10] γ_3 is negative. We note that our values of γ_1 , γ_2 and γ_3 extracted from fitting the excitonic fine structure may serve as benchmark for further improvement of computational methods.

[1] G. F. Koster, R. G. Wheeler, J. O. Dimmock, H. Statz. *Properties of the thirty-two point groups* (MIT Press, 1963).
[2] C. Uihlein, D. Fröhlich, R. Kenkies. *Investigation of exciton fine structure in Cu₂O*. Phys. Rev. B **23**, 2731 (1981).
[3] A. Abragam, B. Bleaney. *Electron paramagnetic resonance of transition ions*. International series of monographs on physics (Clarendon P., 1970).
[4] A. Baldereschi, N. Lipari. *Spherical Model of Shallow Acceptor States in Semiconductors*. Phys. Rev. B **8**, 2697 (1973).

[5] D. A. Varshalovich, A. N. Moskalev, V. K. Khersonskii. *Quantum Theory of Angular Momentum* (World Scientific Publishing, 1988).
[6] A. Baldereschi, N. O. Lipari. *Cubic contributions to the spherical model of shallow acceptor states*. Phys. Rev. B **9**, 1525 (1974).
[7] N. Lipari, A. Baldereschi. *Interpretation of acceptor spectra in semiconductors*. Solid State Communications **25**, 665 (1978).
[8] E. L. Ivchenko. *Optical spectroscopy of semiconductor nanostructures* (Alpha Science, Harrow UK, 2005).
[9] M. French, R. Schwartz, H. Stolz, R. Redmer. *Electronic*

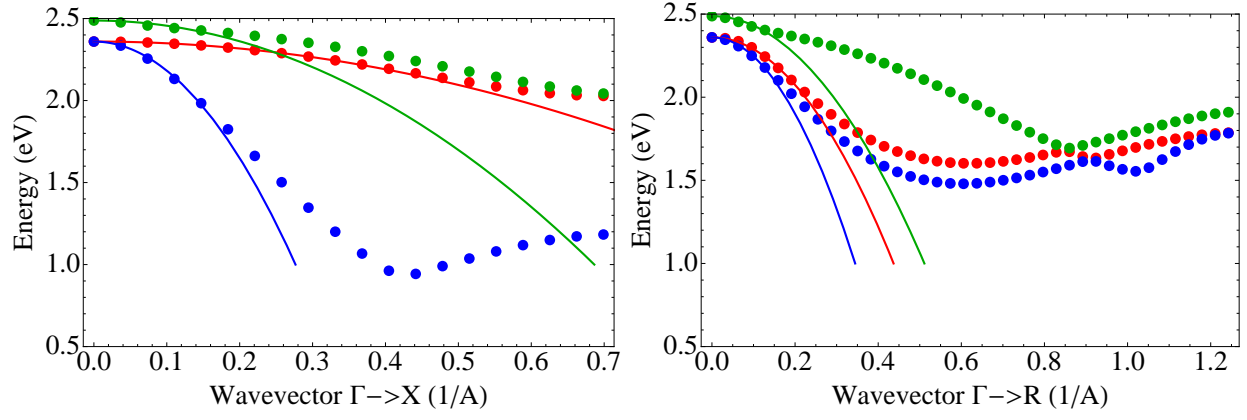


Figure 6: Fit of the DFT band structure along the [001] and [111] axes [9].

band structure of Cu_2O by spin density functional theory. *Journal of Physics: Condensed Matter* **21**, 015502 (2009).

- [10] E. Ruiz, S. Alvarez, P. Alemany, R. A. Evarestov. *Electronic structure and properties of Cu_2O* . *Phys. Rev. B* **56**, 7189 (1997).
- [11] In derivation of Eqs. (6a) and (7) one has to take into account that the hole spin representation is Γ_7^+ (while a

real spin 1/2 transforms according to Γ_6^+ .

- [12] Parts of these equations (for $F = 5/2$ and restricted to the Γ_8^+ representation) were derived in Ref. [6] for the problem of an acceptor. Note that there are two minor misprints in Ref. [6]: in the last element of Eq. (18b) they give 34/115 instead of 34/175 and in the expression for one of the $9j$ symbols they give the middle line as 1 1 1 instead of 1 1 2.